OXFORD

## RESEARCH ARTICLE

# Neurokinin-3 Receptor Binding in Guinea Pig, Monkey, and Human Brain: In Vitro and in Vivo Imaging Using the Novel Radioligand, [18F]Lu AF10628

Katarina Varnäs, PhD; Sjoerd J. Finnema, PhD; Vladimir Stepanov, PhD; Akihiro Takano, MD, PhD; Miklós Tóth, PhD; Marie Svedberg, PhD; Søren Møller Nielsen, PhD; Nikolay A. Khanzhin, PhD; Karsten Juhl, PhD; Benny Bang-Andersen, PhD; Christer Halldin, PhD; Lars Farde, MD, PhD

Karolinska Institutet, Department of Clinical Neuroscience, Centre for Psychiatry Research, Stockholm, Sweden (Drs Varnäs, Finnema, Stepanov, Takano, Tóth, Svedberg, Halldin, and Farde); Lundbeck Research, H. Lundbeck A/S, 9 Ottiliavej, DK-2500 Copenhagen-Valby, Denmark (Drs Møller Nielsen, Khanzhin, Juhl, and Bang-Andersen); AstraZeneca Translational Science Centre at Karolinska Institutet, PET CoE, Stockholm, Sweden (Dr Farde).
Present address: Glycom A/S, Diplomvej 373, 1, DK-2800 Kgs. Lyngby, Denmark (N.A.K.).

Correspondence: Katarina Varnäs, PhD, Karolinska Institutet, Department of Clinical Neuroscience, Centre for Psychiatry Research, R5:02 Karolinska University Hospital, SE-17176 Stockholm, Sweden (katarina.varnas@ki.se).

## Abstract

**Background:** Previous autoradiography studies have suggested a marked interspecies variation in the neuroanatomical localization and expression levels of the neurokinin 3 receptor, with high density in the brain of rat, gerbil, and guinea pig, but at the time offered no conclusive evidence for its presence in the human brain. Hitherto available radioligands have displayed low affinity for the human neurokinin 3 receptor relative to the rodent homologue and may thus not be optimal for cross-species analyses of the expression of this protein.
**Methods:** A novel neurokinin 3 receptor radioligand, [18F]Lu AF10628 ((S)-N-(cyclobutyl(3-fluorophenyl)methyl)-8-fluoro-2-((3-[18F]-fluoropropyl)amino)-3-methyl-1-oxo-1,2-dihydroisoquinoline-4-carboxamide), was synthesized and used for autoradiography studies in cryosections from guinea pig, monkey, and human brain as well as for positron emission tomography studies in guinea pig and monkey.
**Results:** The results confirmed previous observations of interspecies variation in the neurokinin 3 receptor brain localization with more extensive distribution in guinea pig than in primate brain. In the human brain, specific binding to the neurokinin 3 receptor was highest in the amygdala and in the hypothalamus and very low in other regions examined. Positron emission tomography imaging showed a pattern consistent with that observed using autoradiography. The radioactivity was, however, found to accumulate in skull bone, which limits the use of this radioligand for in vivo quantification of neurokinin 3 receptor binding.

**Conclusion:** Species differences in the brain distribution of neurokinin 3 receptors should be considered when using animal models for predicting human neurokinin 3 receptor pharmacology. For positron emission tomography imaging of brain neurokinin 3 receptors, additional work is required to develop a radioligand with more favorable in vivo properties.

**Keywords:** autoradiography, positron emission tomography, tachykinin receptor, $NK_3$ receptor

## Introduction

The tachykinins, substance P, neurokinin A, and neurokinin B (NKB) constitute a group of peptide neurotransmitters that are known to bind to 3 G protein-coupled receptor subtypes, the $NK_1$, $NK_2$, and $NK_3$ receptors (Gerard et al., 1993). These neuropeptides and receptors have long been thought to be implicated in the pathophysiology and putative treatment of a range of CNS disorders (Hökfelt et al., 1980; Pantaleo et al., 2010).

The $NK_3$ receptor has attracted particular attention as a potential target for the treatment of psychiatric disorders such as schizophrenia (Spooren et al., 2005; Dawson and Porter, 2013). In preclinical studies, $NK_3$ receptor agonists have been shown to have a stimulatory effect on dopaminergic neurotransmission (Keegan et al., 1992; Seabrook et al., 1995; Alonso et al., 1996; Nalivaiko et al., 1997; Marco et al., 1998), whereas $NK_3$ receptor antagonists inhibit drug-induced dopaminergic cell firing (Gueudet et al., 1999) and dopamine release (Dawson et al., 2008), supporting potential utility of these agents in the treatment of psychosis.

The notion that $NK_3$ receptor antagonists may have antipsychotic properties has, however, not been supported by clinical trials. Though initial evidence for antipsychotic efficacy was reported for the $NK_3$ receptor antagonist osanetant (Meltzer et al., 2004), subsequent studies with osanetant and 2 additional $NK_3$ receptor antagonists, talnetant and AZD2624, have failed to demonstrate clinical efficacy in the treatment of schizophrenia (Griebel and Beeske, 2012; Dawson and Porter, 2013). However, available data regarding the therapeutic potential of $NK_3$ receptor antagonists for the treatment of psychiatric disorders remain inconclusive. First, given the lack of a suitable positron emission tomography (PET) radioligand for $NK_3$ receptors, it is not known whether sufficient receptor occupancy had been achieved in the clinical trials. Second, information regarding the anatomical localization of $NK_3$ receptors in the human brain is limited, and it is therefore not known whether initial findings in animal models can be extrapolated to human conditions.

Translational research on the $NK_3$ receptor has indeed been hampered by species differences in pharmacology (Maggi, 1995) and receptor distribution patterns (Dietl and Palacios, 1991; Langlois et al., 2001; Rigby et al., 2005). Whereas previous autoradiography studies using $^{125}$I-labeled eledoisin (a peptide analogue of NKB derived from mollusks) as a radioligand have demonstrated high density of $NK_3$ receptors in the brain of rat, gerbil, and guinea pig, no evidence has been obtained for binding of radiolabeled eledoisin analogues to $NK_3$ receptors in the human brain (Dietl and Palacios, 1991; Rigby et al., 2005). An autoradiographic study using the radioligand [$^3$H]senktide has, however, provided support for binding to human brain $NK_3$ receptors, although only data for frontal and sensorimotor cortices were reported (Mileusnic et al., 1999). The presence of $NK_3$ receptors in the primate brain has also been supported by evidence of $NK_3$ mRNA expression, as detected using the polymerase chain reaction, in several regions of the monkey (Nagano et al., 2006) and human brain (Buell et al., 1992) and by immunohistochemistry studies, suggesting expression of $NK_3$ receptors in the human

hypothalamus, cortex, and hippocampus (Mileusnic et al., 1999; Koutcherov et al., 2000; Tooney et al., 2000).

The lack of binding in early autoradiography studies using human brain tissue could possibly be explained by limitations of $^{125}$I-labeled eledoisin as a radioligand, having suboptimal affinity for human $NK_3$ receptors. Thus, the affinity of eledoisin for human $NK_3$ receptors ($K_i$ >300nM; Buell et al., 1992) has been reported to be more than 10-fold lower than for rat (19nM; Bergström et al., 1987) and guinea pig (35nM; Guard et al., 1990). In addition to the low affinity for human $NK_3$ receptors, susceptibility of the radioligand to degradation by peptidases in brain tissue could contribute to the lack of a detectable signal (Dietl and Palacios, 1991; Rigby et al., 2005).

In the present study, [$^{18}$F]Lu AF10628 ((S)-N-(cyclobutyl(3-fluorophenyl)methyl)-8-fluoro-2-((3-[$^{18}$F]-fluoropropyl)amino)-3-methyl-1-oxo-1,2-dihydroisoquinoline-4-carboxamide), a selective nonpeptide $NK_3$ receptor antagonist radioligand with high affinity across species, was used to examine the anatomical distribution of $NK_3$ receptors. The positron emitting isotope $^{18}$F offers the advantage of high image resolution, combined with a relatively long half-life (approximately 110 minutes) and thereby allows for in vitro and in vivo imaging with autoradiography and PET using the same radioligand. Autoradiography studies in guinea pig, monkey, and human brain tissue was used for the interspecies comparison, as this radioligand has been found to have similar affinity for guinea pig and primate $NK_3$ receptors ($K_i$ values of 0.21 and 0.24nM for guinea pig and human receptors, respectively; for details, see supplementary Material). In addition, the in vivo properties of [$^{18}$F]Lu AF10628 as a PET radioligand for brain $NK_3$ receptors were characterized in guinea pig and monkey.

## Methods

### Radiochemistry

Lu AF10628 and (S)-N-(cyclopropyl(4-fluorophenyl)methyl)-2-(ethylamino)-8-fluoro-3-methyl-1-oxo-1,2-dihydroiso-quinoline-4-carboxamide as well as the precursor, (S)-3-((tert-butoxycarbonyl)(4-((cyclobutyl(3-fluorophenyl)methyl)carbamoyl)-8-fluoro-3-methyl-1-oxoisoquinolin-2(1H)-yl)amino)propyl 4-methylbenzenesulfonate, for synthesis of [$^{18}$F]Lu AF10628 were synthesized at H. Lundbeck A/S, Copenhagen-Valby, Denmark. Other compounds and chemicals were obtained from commercially available sources and were of analytical grade wherever possible. [$^{18}$F]Lu AF10628 (Figure 1) was synthesized and purified using a semiautomatic synthesis module (DM Automation). [$^{18}$F]Fluoride was produced via the $^{18}$O(p,n)$^{18}$F nuclear reaction using a GE Medical Systems PETtrace cyclotron with a silver liquid water target. The radionuclide was then trapped on a QMA Light Sep-Pak cartridge (bicarbonate form), and [$^{18}$F]fluoride was eluted into the reaction vessel using 2mL of acetonitrile/water (96/4 vol/vol) containing 9.8mg of Kryptofix 2.2.2 and 1.8mg of potassium carbonate. The solvent was then
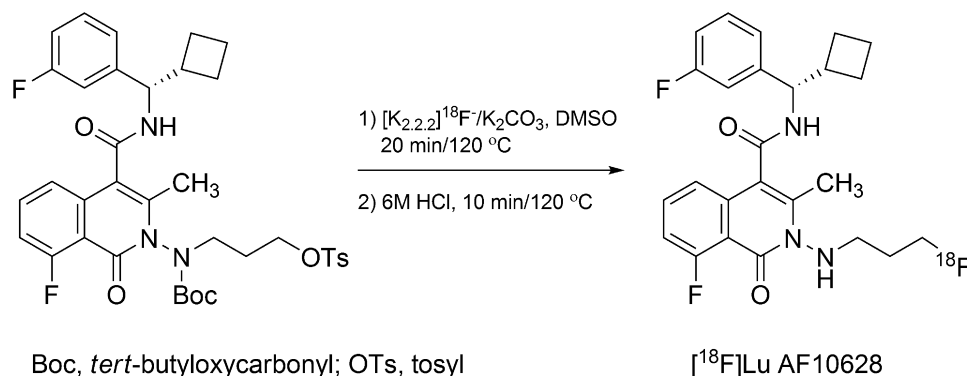
**Figure 1.** Radiosynthesis of [$^{18}$F]Lu AF10628.

evaporated by heating at 140°C under a stream of nitrogen (100 mL/min). To the dried [$^{18}$F]fluoride/Kryptofix complex, 0.5 to 0.7 mg of (S)-3-((*tert*-butoxycarbonyl)(4-((cyclobutyl(3-fluorophenyl)methyl)carbamoyl)-8-fluoro-3-methyl-1-oxoisoquinolin-2(1*H*)-yl)amino)propyl 4-methylbenzenesulfonate dissolved in 500–600 μL of *N,N*-dimethylformamide was added. The reaction mixture was heated for 20 minutes at 120°C in a glass reactor without stirring. After 20 minutes, the reactor was cooled to room temperature and 200 to 300 μL of 6M aq. hydrochloric acid was added and reaction mixture heated for 120°C for another 10 minutes. After deprotection, the reaction mixture was diluted with water and the crude product was injected directly onto semipreparative HPLC column, Waters μBondapak C18 column (10 μm, 125 A, 7.8 × 300 mm), and purified using HPLS system consisting of the following components: Smartline Pump 100 (Knauer), automatic sample injector (Rheodyne-type) with a 2-mL loop; Smartline UV Detector 2500 (Knauer) and a gamma-radioactivity PIN diode detector (Caroll & Ramsey Associates) using acetonitrile-water 450:550 mixture as the mobile phase with flow of 6 mL/min, with UV detector set to 254 nm. The desired fraction was collected into a vial containing 50 mL of water. The resulting solution was pushed through a Sep-Pak tC18 Plus Short cartridge; after trapping of the product the cartridge was rinsed with 10 mL of distilled water, and the product ([$^{18}$F]Lu AF10628) was then eluted with approximately 1 mL of ethanol and collected in a sterile receiving vial prefilled with 9 to 10 mL of sterile phosphate buffered saline. Finally, the product was passed through a sterile filter (0.22-μm pore size, Millipore) in a clean-room environment.

The radiochemical purity of [$^{18}$F]Lu AF10628 was determined using analytical radio-HPLC under the following conditions: C-18 μBondapak analytical column (3.9 × 300 mm, 5 μm, acetonitrile:water 60:40, flow 2 mL/min, UV 254 nm). The identity of [$^{18}$F]Lu AF10628 was confirmed by co-injection with an authentic nonradioactive standard. [$^{18}$F]Lu AF10628 was produced with sufficient radiochemical yield (10–30%, decay corrected), high specific radioactivity (>2000 Ci/mmol), and high radiochemical purity (>95.0%). The total amount of unknown chemical impurities present in the formulation was <2 μg/injection.

## In Vitro Autoradiography Studies

### Brain Tissue

Studies using experimental animals were approved by the Animal Ethics Committee of the Swedish Animal Welfare Agency (registration no. 4820/06-600 and 399/08). Studies including human brain tissue were approved by the Ethics Committee at Karolinska Institutet (registration no. 03-767) and the Semmelweis University Human Ethical Committee (registration no. 113/1995, 180/2001).

Brain tissue from 6 guinea pigs and 6 cynomolgus monkeys (*Macaca fascicularis*) was used in the study. The brains were frozen in dry ice-cooled isopentane (-40°C) and stored at -25°C until use. For detailed anatomical analyses, brains were cut at 10 μm (guinea pig brain tissue; n = 2) and 20 μm (monkey brain tissue; n = 3) coronal and sagittal sections on a freezing microtome (Leica, Heidelberg, Germany) and thaw mounted onto gelatin-coated slides. In addition, for quantitative analyses comparing radioligand binding density across species, brain tissue from 4 guinea pigs and 3 monkeys were sectioned, using a freezing microtome (Leica, Heidelberg, Germany), into 100–μm-thick sections.

Human brains were obtained at clinical autopsy at the National Institute of Forensic Medicine, Karolinska Institutet (Stockholm, Sweden) and the Department of Forensic Medicine, Semmelweis Medical University, Budapest, Hungary. Whole hemispheres were removed, frozen, and cryosectioned in accordance with previously described procedures (Hall et al., 1998), using a heavy-duty cryomicrotome (Leica cryomacrocut CM3600, Leica, Nussloch, Germany). Tissue was obtained from 2 male and 1 female donor (ages 32, 58, and 59 years) with no known neurological or psychiatric diagnosis at the time of death. The postmortem times ranged between 11 and 15 hours. From examination at autopsy and during sectioning, none of the brains exhibited damage, abnormalities, or neurologic features. The whole hemispheres were oriented so that a line connecting the anterior and posterior commissures was parallel to the surface of the cryostat specimen holder. Subsequently, whole hemispheres were cryosectioned into 100-μm-thick coronal or horizontal cryosections, transferred to gelatinized glass plates (10–22 cm), dried at room temperature, and then stored with dehydrating agents (-25°C) until use.

In addition to the above-mentioned whole hemisphere brain cryosections, the other human brain specimens had been obtained at autopsy. The tissue was immediately cut into coronal slabs, frozen in dry-ice-cooled isopentane, and stored at -70°C. The slabs were subsequently cut into coronal blocks of tissue containing the brainstem. Twenty-micron-thick cryosections were taken from these blocks using a Leica cryostat (Heidelberg, Germany), dried onto glass slides, and stored frozen at -70°C until later use.

### Autoradiography

Autoradiography was carried out essentially as described earlier (Hall et al., 1998). The sections were preincubated at room temperature for 5 minutes in Tris-HCl buffer (pH 7.4, 50 mM).

Subsequently, the sections were incubated for 90 minutes at room temperature with [18F]Lu AF10628 (0.02 MBq/mL) in Tris-HCl buffer (pH 7.4, 50 mM) containing 3 mM $MnCl_2$. After incubation, sections were washed with cold Tris buffer (pH 7.4, 50 mM; 3 x 30 minutes for whole hemisphere sections and 3 x 5 minutes for sections from smaller tissue blocks), briefly dipped into distilled water, and dried on a warm plate.

Nonspecific binding was defined in adjacent sections co-incubated with 10 μM osanetant. Specificity and selectivity of the binding were further assessed in a series of consecutive sections incubated in the absence and presence of the selective $NK_3$ receptor antagonists SB222200 (100 nM; Sarau et al., 2000) or (S)-N-(cyclopropyl(4-fluorophenyl)methyl)-2-(ethylamino)-8-fluoro-3-methyl-1-oxo-1,2-dihydroisoquinoline-4-carboxamide (100 nM), respectively, or the $NK_2$ receptor selective antagonist saredutant (100 nM; Emonds-Alt et al., 1992).

Radioactivity was detected and quantified with a phosphor imager (Fuji BAS-5000 image reader). Brain regions of interest (ROI) were defined in autoradiography images with reference to brain anatomical atlases (Rapisarda and Bacchelli, 1977; Mikula et al., 2007; Mai et al., 2008). Nuclei of amygdala were defined according to the description by Yilmazer-Hanke (2012). The measured photostimulated luminescence/mm² values were subsequently transformed into radioactivity units (kBq/mm³) based on intensity values obtained using radioactivity standards from serial dilutions of the incubation solution assuming that the volume of the region of interest was the product of the area and section thickness (100 μm). Finally, specific binding was calculated by subtracting nonspecific binding, defined in the presence of 10 μM osanetant, from the total [18F]Lu AF10628 binding.

## PET Studies in Guinea Pig and Monkey

Studies in guinea pigs were conducted in accordance with the guidelines of the Swedish National Board of Laboratory Animals and Karolinska Institutet's guidelines for planning, conducting, and documenting experimental research (registration no. 4820/06-600) under protocols approved by the Animal Ethics Review Board of Northern Stockholm, Sweden (N557/11). Two Dunkin Hartley guinea pigs, weighing 0.84 and 0.85 kg, respectively, obtained from Harlan Laboratories were housed at the animal department of Karolinska University Hospital in a temperature- (approx. 21°C) and humidity- (approximately 40%) controlled environment on a 12-h-light/-dark cycle (lights on 7:00 AM) with access to food and water ad libitum. Animals were allowed at least 1 week to habituate to the animal department before start of the imaging sessions.

All experiments were conducted during the light phase of the cycle. The imaging experiments were performed under isoflurane anesthesia (induction: 4%-5%, maintenance: 1.5%-2% in 50/50 air/oxygen). [18F]Lu AF10628 (16.8 and 16.9 MBq, respectively) was injected i.v. into the 2 guinea pigs. Radioactivity was measured for 123 minutes according to a preprogrammed series of 35 frames, using the small-animal nanoScan PET/CT and PET/MRI systems (Mediso Ltd.; Szanda et al., 2011; Nagy et al., 2013) at Karolinska Experimental Research Imaging Center.

The PET study in nonhuman primates was approved by the Animal Ethics Committee of the Swedish Animal Welfare Agency (registration no. 399/08) and was performed according to the "Guidelines for planning, conducting and documenting experimental research" (registration no. 4820/06-600) of Karolinska Institutet as well as the "Guide for the Care and Use of Laboratory Animals" (Clark et al., 1997).

Two cynomolgus monkeys weighing 4.0 and 6.3 kg, respectively, were supplied by Astrid Fagraeus Laboratory, Karolinska Institutet, Solna, Sweden. MRIs of the monkey brains were obtained using a 1.5 T General Electrics Signa (GE, Milwakee, WI) system. A spoiled gradient recalled sequence was acquired in the coronal plane with the following parameters: TR=21 ms; TE=4 ms; flip angle=35°; slice thickness=1.0 mm; FOV=12.8 cm; NEX=2; voxel size = 0.5 x 0.5 x 1 mm³.

Anesthesia was induced by i.m. injection of ketamine hydrochloride (approximately 10 mg/kg) and maintained after endotracheal intubation by administration of a mixture of sevoflurane, oxygen, and medical air. The monkey was observed continuously during the PET experimental day. Body temperature was maintained by Bair Hugger Model 505 (Arizant Healthcare Inc.) and monitored by an esophageal thermometer. Electrocardiogram, heart rate, respiratory rate, oxygen saturation, and arterial blood pressure were continuously monitored throughout the experiment. No anesthesia- or drug-related effects on vital parameters were noted. A head fixation system was used to secure a fixed position of the monkey's head throughout the PET measurement (Karlsson et al., 1993).

A sterile physiological phosphate buffer (pH=7.4) solution of [18F]Lu AF10628 (153 or 157 MBq) was injected as a bolus into a sural vein during 5 seconds with simultaneous start of PET-data acquisition. The PET measurement was conducted using the High Resolution Research Tomograph (Siemens Molecular Imaging, Knoxville, TN). List mode data were reconstructed using the ordinary Poisson-3D-ordered subset expectation maximization algorithm, with 10 iterations and 160 subsets including modeling of the point spread function. The corresponding in-plane resolution with ordinary Poisson-3D-ordered subset expectation maximization point spread function was 1.5 mm in the center of the field of view and 2.4 mm at 10-cm off-center directions (Varrone et al., 2009). Attenuation correction was acquired with a 6-minute transmission measurement using a single 137Cs source. List-mode data were acquired continuously for 180 minutes starting at the time of radioligand injection. Positron emission tomography images were then reconstructed with a series of 28 frames.

Venous blood samples (2 mL) were obtained manually at 5, 30, 60, 90, 120, and 150 min after injection of [18F]Lu AF10628 in the monkeys. After centrifugation, 0.5 to 0.8 mL plasma was pipetted and plasma radioactivity was measured in a well counter (Farde et al., 1989). The fraction of plasma radioactivity corresponding to unchanged radioligand in plasma was determined as previously described for other PET radioligands (Halldin et al., 2001). Briefly, venous plasma samples were deproteinized with acetonitrile and analyzed by gradient HPLC with radiodetection.

Coregistrations and ROI delineations were performed using PMOD v. 3 (Pixel-wise modeling software, PMOD Group, Zurich, Switzerland). For guinea pigs, ROIs were delineated for the cortex, amygdala, cerebellum, caudate-putamen, thalamus, the whole brain, and skull on a guinea pig brain T2-weighted MRI, which was used as a template for manual coregistration of PET images. The monkey brain MRI was manually coregistered to the average PET image and ROIs for skull, temporal cortex, amygdala, cerebellum, putamen, thalamus and the whole brain contour were delineated with reference to the coregistered MRI.

The ROIs were displayed on the corresponding PET images and pair-wise pooled for each anatomical region. Regional radioactivity was calculated for the sequence of time frames, corrected for radioactivity decay, and plotted vs time. For each region a time-radioactivity curve was generated and the radioactivity concentration expressed as kBq/cm³. Regional

radioactivity was normalized to injected radioactivity and body weight and expressed as standard uptake value ([SUV] fraction of injected radioactivity/cm$^3$ brain x body weight [g]).

## Results

### In Vitro Autoradiography Studies

Autoradiographic images of [$^{18}$F]Lu AF10628 binding in brain tissue of guinea pig, monkey, and human are shown in Figure 2. In tissue sections incubated with [$^{18}$F]Lu AF10628, a markedly higher image intensity was observed for the cerebral cortex of guinea pig than for primates (Figure 2A,C,E). Nonspecific binding, as determined in adjacent sections in the presence of the NK$_3$ receptor antagonist osanetant (10 μM), was low and homogeneously distributed (Figure 2B,D,F).

The density of regional specific binding for the 3 species is presented in Table 1. In the guinea pig brain, high [$^{18}$F]Lu AF10628 binding was observed in isocortical regions and the amygdala, with low binding in other regions. In monkey brain tissue, the binding was homogeneously distributed with no evident differences observed between the forebrain regions examined, although the cortical binding displayed a laminar pattern with more intense binding in internal layers (Figure 2C). In the human brain, specific binding was very low in most of the regions analyzed, with exception for the amygdala, which showed intense binding of [$^{18}$F]Lu AF10628. For all of the species investigated, a very low level of specific binding was obtained for the hippocampus, striatum, globus pallidus, and cerebellum.

Binding was unevenly distributed among subregions of the human amygdala and was highest in the ventromedial part of the basolateral nucleus and paralaminar nucleus, extending to the parahippocampal-amygdaloid transition area and entorhinal cortex (Figure 3; Table 1). Binding was lower in the medial nucleus and the dorsal part of the basolateral amygdaloid nucleus (Figure 3).

Specific binding, defined as the difference between total [$^{18}$F]Lu AF10628 binding and the binding remaining in the presence of 10 μM osanetant, was moderate (approximately 0.4 kBq/mm$^3$) in the human hypothalamus (paraventricular and supraoptic nuclei; Figures 2E and 3) and low (0.15–0.16 kBq/mm$^3$) in the bed nucleus of stria terminalis and the basal nucleus of Meynert
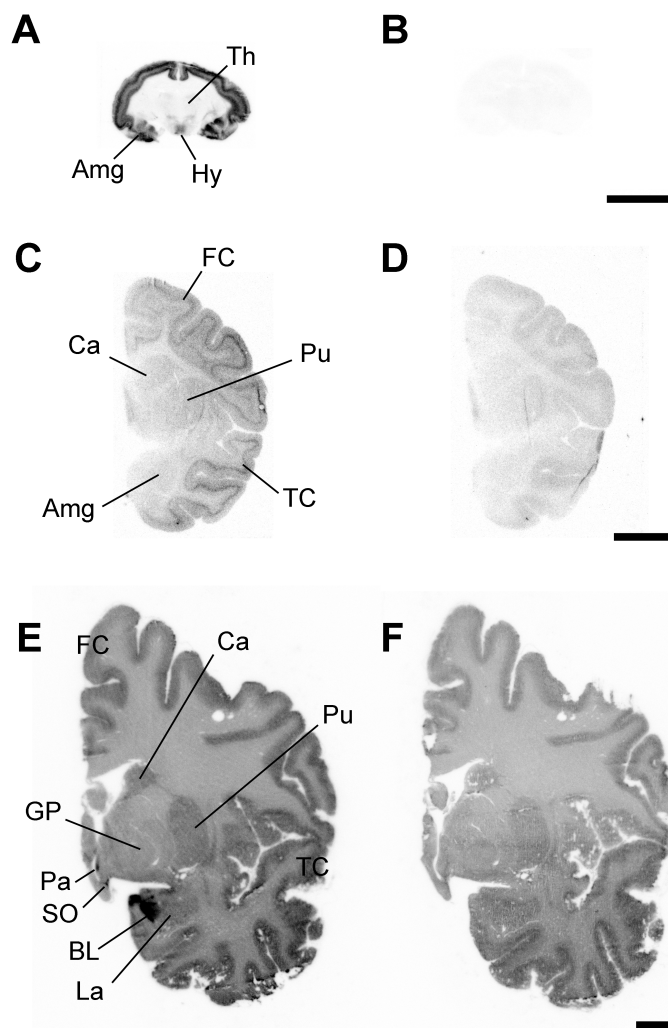


**Figure 2.** Autoradiograms showing binding of [$^{18}$F]Lu AF10628 to neurokinin 3 (NK$_3$) receptors in coronal sections of the guinea pig (A-B), monkey (C-D), and human brain (E-F). Total binding (A, C, E) and nonspecific binding in the presence of the NK$_3$ receptor compound osanetant (10 μM; B, D, F). Amg, amygdaloid nuclei; BL, basolateral amygdaloid nucleus; Ca, caudate nucleus; FC, frontal cortex; GP, globus pallidus; Hy, hypothalamus; La, lateral amygdaloid nucleus; Pa, paraventricular nucleus of the hypothalamus; Pu, putamen; SO, supraoptic nucleus of the hypothalamus; TC, temporal cortex; Th, thalamus. Scale bar = 1 cm.

**Table 1.** Binding of [18F]Lu AF10628 to NK$_3$ Receptors In Autoradiography Studies of the Guinea Pig, Monkey, and Human Brain

| Region | Guinea Pig | | | Monkey | | | Human | | |
|---|---|---|---|---|---|---|---|---|---|
| | n | Mean | Range | n | Mean | Range | n | Mean | Range |
| Amygdala | 4 | 1.1 | 1.0–1.1 | 3 | 0.10 | 0.08–0.12 | | | |
|   Basolateral nucleus, ventromedial part | | | | | | | 3 | 1.1 | 0.93–1.2 |
|   Lateral nucleus | | | | | | | 3 | 0.09 | 0.04–0.15 |
| Cortex | 4 | 1.4 | 1.2–1.6 | | | | | | |
|   Frontal | | | | 1 | 0.13 | | 3 | 0.05 | 0.03–0.09 |
|   Temporal | | | | 3 | 0.12 | 0.12–0.13 | 3 | 0.09 | 0.02–0.16 |
|   Occipital | | | | 3 | 0.17 | 0.13–0.21 | 1 | 0.05 | |
| Striatum | 2 | 0.11 | 0.05–0.17 | 3 | 0.08 | 0.07–0.09 | | | |
|   Caudate nucleus | | | | | | | 3 | 0.06 | 0.05–0.08 |
|   Putamen | | | | | | | 3 | 0.05 | 0.03–0.09 |
| Thalamus | 4 | 0.21 | 0.18–0.24 | 1 | 0.14 | | 3 | 0.04 | 0.01–0.09 |
| Hippocampus | 2 | 0.02 | 0.00–0.04 | 3 | 0.07 | 0.05–0.08 | 3 | 0.06 | 0.01–0.09 |
| Substantia nigra | 2 | 0.20 | 0.17–0.24 | 3 | 0.10 | 0.09–0.11 | 1 | 0.10 | |
| Cerebellum | 4 | 0.09 | 0.03–0.12 | 3 | 0.08 | 0.08-0.08 | 1 | 0.05 | |

Radioactivity concentration expressed in kBq/mm$^3$ tissue.
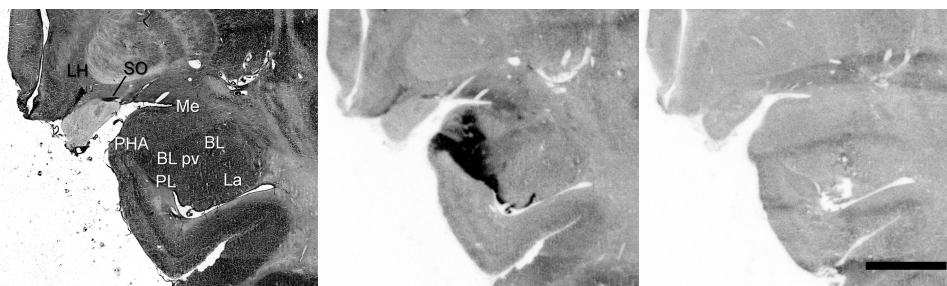


**Figure 3.** Details of human brain whole hemisphere autoradiograms showing binding of the neurokinin 3 (NK$_3$) receptor antagonist [18F]Lu AF10628 in the amygdala and hypothalamus. Cresyl violet stained section (left), total binding (middle), and nonspecific binding in the presence of the NK$_3$ receptor compound osanetant (10 µM; right). BL, basolateral amygdaloid nucleus; BL pv, basolateral amygdaloid nucleus, parvicellular part; La, lateral amygdaloid nucleus; LH, lateral hypothalamic area; Me, medial amygdaloid nucleus; PHA, parahippocampal-amygdaloid transition area; PL, paralaminar amygdaloid nucleus; SO, supraoptic nucleus of the hypothalamus. Scale bar = 1 cm.

(results not shown). Very low specific binding was observed in cortical regions (frontal, temporal, insular, cingulate, and occipital cortex; Table 1) and in the brainstem substantia nigra (supplementary Figure 1A-B) and raphe nuclei (supplementary Figure 1C-F).

The selectivity of the binding to human NK$_3$ receptors was examined in adjacent sections co-incubated with the 2 chemically distinct NK$_3$ receptor antagonists, SB222200 and (S)-N-(cyclopropyl(4-fluorophenyl)methyl)-2-(ethylamino)-8-fluoro-3-methyl-1-oxo-1,2-dihydroisoquinoline-4-carboxamide, or with the NK$_2$ receptor selective antagonist saredutant. The binding was inhibited by 100-nM concentrations of SB222200 and (S)-N-(cyclopropyl(4-fluorophenyl)methyl)-2-(ethylamino)-8-fluoro-3-methyl-1-oxo-1,2-dihydroisoquinoline-4-carboxamide, but remained at the same level as the total binding in tissue cryosections co-incubated with 100 nM saredutant (Figure 4A-D).

### PET Studies in Guinea Pig And Monkey

After i.v. administration of [18F]Lu AF10628 in guinea pig, brain radioactivity reached peak concentration within 1 minute (0.90–0.95 SUV) after which it rapidly decreased. A similar time course was seen in monkey, where the maximum brain radioactivity concentration (1.0–1.2 SUV) was reached at 1.5 minutes after radioligand administration.

Images of the averaged radioactivity for the initial 30 minutes after [18F]Lu AF10628 injection showed a pattern of preferential binding in cortical regions of the guinea pig brain, whereas the binding in monkey was homogeneously distributed throughout the brain regions studied (Figure 5). For both species, brain radioactivity was low (<0.7 SUV) at late time (after 30 minutes) of PET data acquisition when a much larger proportion of radioactivity was detected outside the brain within the skull. The pattern of the observed regional radioactivity distribution could be confirmed by time curves for radioactivity in the skull and different brain regions (Figure 6A-B). The ratios of AUC calculated based on 5 to 30 minutes of data acquisition for cortex to the cerebellum were 2.2 (mean; n = 2) and 1.2 (mean; n = 2) for guinea pig and monkey, respectively.

The percentage of parent [18F]Lu AF10628 in monkey plasma was 39% to 45 % at 30 minutes postinjection and 18% to 27 % at 90 minutes postinjection. At 30 minutes after radioligand injection, the average ratio of regional brain radioactivity concentration to that for metabolite corrected plasma was 2.3 for cortex and 1.6 for the cerebellum.

### Discussion

The aim of the present study was to examine and compare the regional localization of NK$_3$ receptors in the brain of 3 species.
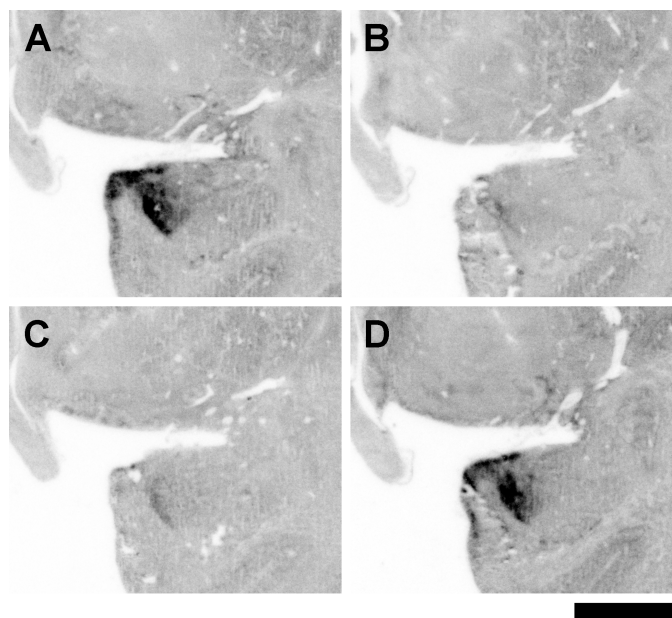
**Figure 4.** Selectivity of [$^{18}$F]Lu AF10628 binding to the human brain neurokinin 3 (NK$_3$) receptor. (A) Total binding. Binding in the presence of saturating concentration (100 nM) of the NK$_3$ receptor-selective compounds SB222200 (B) and (S)-N-(cyclopropyl(4-fluorophenyl)methyl)-2-(ethylamino)-8-fluoro-3-methyl-1-oxo-1,2-dihydroisoquinoline-4-carboxamide (C), respectively, and the NK$_2$ receptor selective compound saredutant (100 nM; D). Scale bar = 1 cm.
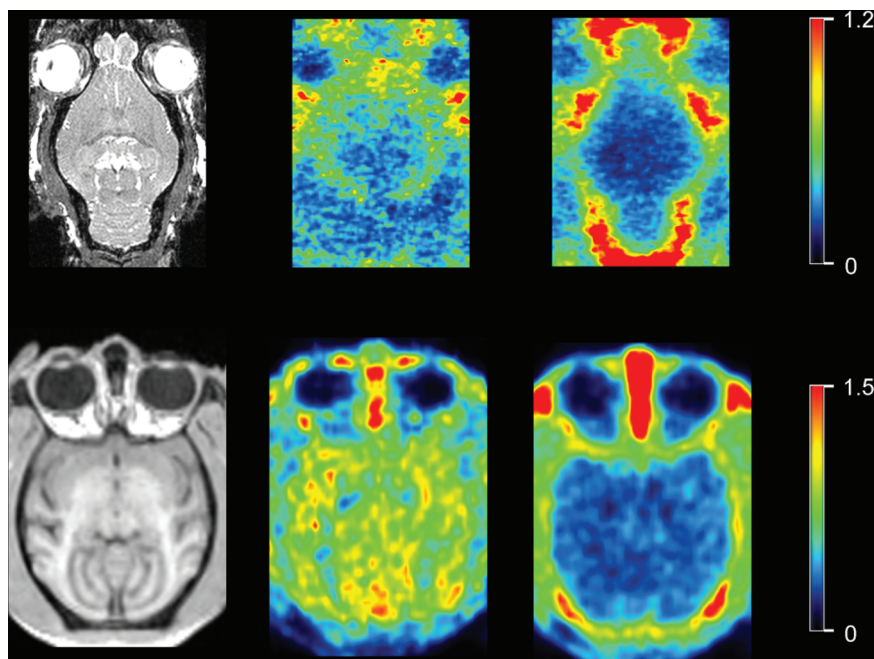


**Figure 5.** Positron emission tomography images of radioactivity in the guinea pig brain (top) and monkey brain (bottom) after i.v. injection of [$^{18}$F]Lu AF10628. The left panel shows the guinea pig MRI template and the individual monkey MR images, respectively, used for anatomical definition of regions of interest. The middle and right panels show average radioactivity from 0 to 30 minutes and 30 to 123 minutes, respectively, after [$^{18}$F]Lu AF10628 injection. Image intensity is presented in SUV units.

The results confirmed previous observations of a marked cross-species variation, with higher density and a more widespread anatomical distribution in guinea pig than in primate brain. However, contrary to previous evidence, specific radioligand binding to the NK$_3$ receptor was obtained also for some human brain regions, notably in specific nuclei of amygdala.

Despite the conspicuous binding in the human amygdala, a correspondingly high binding was not evident in the amygdala of the monkey (Figure 2C; supplementary Figure 2). Conversely, a layer-specific cortical binding pattern, consistent with that previously reported using autoradiography in nonhuman primate brain (Rigby et al., 2005), was found for monkey but was not identified in human tissue sections. This discrepancy is unexpected given the close agreement in binding patterns commonly reported for other neurotransmitter receptors in the human and nonhuman primate brain. Given that no information is available
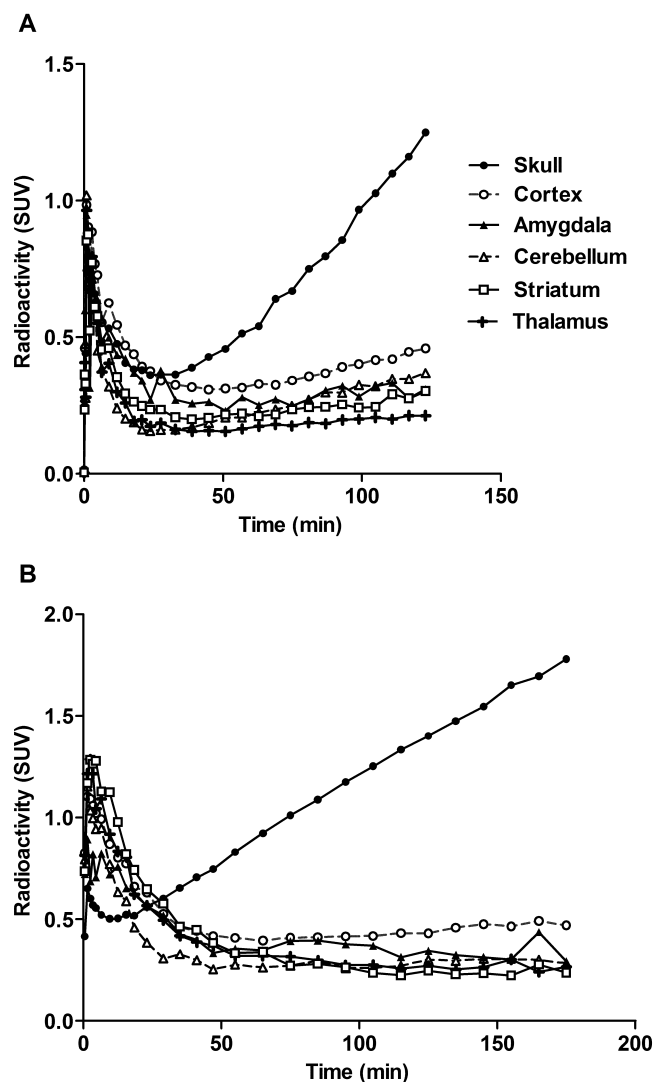
**A**



**B**



**Figure 6.** Time curves for radioactivity in brain regions and skull after administration of [¹⁸F]Lu AF10628 in guinea pig (A) and monkey (B).

regarding the affinity of Lu AF10628 for monkey $NK_3$ receptors, it is possible that the discrepant binding patterns observed may reflect species differences in affinity between monkey and human receptors. However, this interpretation seems unlikely, based on similar amino acid sequence (Nagano et al., 2006), and affinity of established $NK_3$ receptor compounds (Nagano et al., 2006; Malherbe et al. 2011), for nonhuman primate and human $NK_3$ receptors. Nevertheless, the unique binding pattern observed in the cerebral cortex supports that [¹⁸F]Lu AF10628 binds specifically to monkey $NK_3$ receptors under the present experimental conditions.

To analyze the binding to brain $NK_3$ receptors, a novel radioligand, [¹⁸F]Lu AF10628, was used as the imaging tool. Lu AF10628 was selected from a chemical series where in vitro affinities for the $NK_1$ receptor in general were in the micromolar range and where high selectivity vs other targets was observed. The in vitro $K_i$ value at the human $NK_2$ receptor was 1 μM, but this specific compound has not been tested for $NK_1$ receptor affinity. In support of selective labeling of $NK_3$ receptors in guinea pig brain, the binding pattern showed a good correspondence with that found using other $NK_3$ receptor radioligands in this species (Langlois et al., 2001; Rigby et al., 2005). Further, selectivity of the

signal for human $NK_3$ vs $NK_2$ receptors was confirmed by the observation that the binding could be inhibited by 2 chemically distinct $NK_3$ receptor ligands, but remained at the same level in the presence of a saturating concentration of an $NK_2$ receptor selective compound. The findings support that the binding pattern observed with [¹⁸F]Lu AF10628 corresponds to the regional distribution of $NK_3$ receptors in brain.

To our knowledge, this study provides the first detailed autoradiographic mapping of the presence of $NK_3$ receptors in human brain. The findings corroborate previous results from immunohistochemistry studies indicating the presence of $NK_3$ receptors in several regions of the human brain, including hypothalamus, hippocampus, and cortex (Mileusnic et al., 1999; Koutcherov et al., 2000; Tooney et al., 2000). In general, immunohistochemistry studies may be limited by lack of specificity of antibodies for the target protein. For instance, the $NK_3$ receptor antibody may show potential cross-reactivity with a kappa-like opioid receptor given sequence similarity with this receptor (Mileusnic et al., 1999). Confirmation of the findings with autoradiography studies using a selective $NK_3$ receptor radioligand now provides conclusive support for the presence of $NK_3$ receptors in human brain.

However, previous studies using $^{125}$I-labeled eledoisin as a radioligand have reported no evidence for binding to NK$_3$ receptors in human brain cryosections (Dietl and Palacios, 1991; Rigby et al., 2005). A likely explanation for the different findings could be the superior properties of [$^{18}$F]Lu AF10628 as a radioligand in terms of affinity for human NK$_3$ receptors (K$_i$ = 0.24 nM for Lu AF10628 vs >300 nM for eledoisin; Buell et al., 1992). A direct comparison of our findings to those in previous studies is not possible, as it is unknown whether the regions showing dense [$^{18}$F] Lu AF10628 binding (amygdala, hypothalamus) were included in the previous studies.

The specific binding of [$^{18}$F]Lu AF10628 in the human hypothalamus was at an intermediate level. The localization of NK$_3$ receptors in this region is consistent with immunohistochemistry findings (Mileusnic et al., 1999; Koutcherov et al., 2000) and with the documented endocrine role of the NKB/NK$_3$ receptor signaling pathway in various species, including human (Topaloglu and Semple, 2011).

The binding was low in brainstem regions of monoaminergic cell bodies, including the substantia nigra and raphe nuclei. This localization pattern found in human brain is thus different from that reported in rats showing notable binding in these nuclei (Langlois et al., 2001; Rigby et al., 2005). The discrepant localization pattern between the rat and human NK$_3$ receptor in these nuclei may serve as a possible explanation for the poor translatability of the preclinical pharmacology of NK$_3$ receptor antagonists to clinical efficacy in CNS disorders.

In PET studies in guinea pig and monkey, the distribution of brain radioactivity was consistent with that found using autoradiography. Thus, the binding was high in the cortex compared with the cerebellum in guinea pig, whereas radioactivity was homogeneously distributed in the monkey brain. However, due to accumulation of radioactivity in the skull and the limited resolution of PET, the signal in brain receives contamination from that in skull at late times of data acquisition, and cannot be accurately quantified. Given the larger intracranial volumes in humans than in preclinical species PET images of the human brain are, to a less extent, affected by contamination of radioactivity from the skull region. Therefore, it cannot be excluded that [$^{18}$F]Lu AF10628 may be suitable for quantitative analysis of brain NK$_3$ receptor binding in humans.

## Acknowledgments

## Statement of Interest

Søren Møller Nielsen, Nikolay A. Khanzhin, Karsten Juhl, and Benny Bang-Andersen are current or past employees of Lundbeck. Lars Farde is employed by AstraZeneca Pharmaceuticals. The other authors declare no conflicts of interest.

## References

Alonso R, Fournier M, Carayon P, Petitpretre G, Le Fur G, Soubrie P (1996) Evidence for modulation of dopamine-neuronal function by tachykinin NK3 receptor stimulation in gerbil mesencephalic cell cultures. Eur J Neurosci 8:801–808.

Bergström L, Torrens Y, Saffroy M, Beaujouan JC, Lavielle S, Chassaing G, Morgat JL, Glowinski J, Marquet A (1987) [$^3$H] neurokinin B and $^{125}$I-Bolton Hunter eledoisin label identical tachykinin binding sites in the rat brain. J Neurochem 48:125–133.

Buell G, Schulz MF, Arkinstall SJ, Maury K, Missotten M, Adami N, Talabot F, Kawashima E (1992) Molecular characterisation, expression and localisation of human neurokinin-3 receptor. FEBS Lett 299:90–95.

Clark JD, Gebhart GF, Gonder JC, Keeling ME, Kohn DF (1997) Special report: the 1996 guide for the care and use of laboratory animals. ILAR J 38:41–48.

Dawson LA, Cato KJ, Scott C, Watson JM, Wood MD, Foxton R, de la Flor R, Jones GA, Kew JN, Cluderay JE, Southam E, Murkitt GS, Gartlon J, Pemberton DJ, Jones DN, Davies CH, Hagan J (2008) In vitro and in vivo characterization of the non-peptide NK3 receptor antagonist SB-223412 (talnetant): potential therapeutic utility in the treatment of schizophrenia. Neuropsychopharmacology 33:1642–1652.

Dawson LA, Porter RA (2013) Progress in the development of neurokinin 3 modulators for the treatment of schizophrenia: molecule development and clinical progress. Future Med Chem 5:1525–1546.

Dietl MM, Palacios JM (1991) Phylogeny of tachykinin receptor localization in the vertebrate central nervous system: apparent absence of neurokinin-2 and neurokinin-3 binding sites in the human brain. Brain Res 539:211–222.

Emonds-Alt X, Vilain P, Goulaouic P, Proietto V, Van Broeck D, Advenier C, Naline E, Neliat G, Le Fur G, Brelière JC (1992) A potent and selective non-peptide antagonist of the neurokinin A (NK$_2$) receptor. Life Sci 50:PL101–106.

Farde L, Eriksson L, Blomquist G, Halldin C (1989) Kinetic analysis of central [$^{11}$C]raclopride binding to D$_2$-dopamine receptors studied by PET--a comparison to the equilibrium analysis. J Cereb Blood Flow Metab 9:696–708.

Gerard NP, Bao L, Xiao-Ping H, Gerard C (1993) Molecular aspects of the tachykinin receptors. Regul Pept 43:21–35.

Griebel G, Beeske S (2012) Is there still a future for neurokinin 3 receptor antagonists as potential drugs for the treatment of psychiatric diseases? Pharmacol Ther 133:116–123.

Guard S, Watson SP, Maggio JE, Too HP, Watling KJ (1990) Pharmacological analysis of [$^3$H]-senktide binding to NK$_3$ tachykinin receptors in guinea-pig ileum longitudinal muscle-myenteric plexus and cerebral cortex membranes. Br J Pharmacol 99:767–773.

Gueudet C, Santucci V, Soubrie P, Le Fur G (1999) Blockade of neurokinin3 receptors antagonizes drug-induced population response and depolarization block of midbrain dopamine neurons in guinea pigs. Synapse 33:71–79.

Hall H, Halldin C, Farde L, Sedvall G (1998) Whole hemisphere autoradiography of the postmortem human brain. Nucl Med Biol 25:715–719.

Halldin C, Gulyas B, Farde L (2001) PET studies with carbon-11 radioligands in neuropsychopharmacological drug development. Curr Pharm Des 7:1907–1929.

Hökfelt T, Johansson O, Ljungdahl A, Lundberg JM, Schultzberg M (1980) Peptidergic neurones. Nature 284:515–521.

Karlsson P, Farde L, Halldin C, Swahn CG, Sedvall G, Foged C, Hansen KT, Skrumsager B (1993) PET examination of [$^{11}$C]NNC 687 and [$^{11}$C]NNC 756 as new radioligands for the D1-dopamine receptor. Psychopharmacology (Berl) 113:149–156.

Keegan KD, Woodruff GN, Pinnock RD (1992) The selective NK3 receptor agonist senktide excites a subpopulation of dopamine-sensitive neurones in the rat substantia nigra pars compacta in vitro. Br J Pharmacol 105:3–5.

Koutcherov Y, Ashwell KW, Paxinos G (2000) The distribution of the neurokinin B receptor in the human and rat hypothalamus. Neuroreport 11:3127–3131.

Langlois X, Wintmolders C, te Riele P, Leysen JE, Jurzak M (2001) Detailed distribution of Neurokinin 3 receptors in the rat, guinea pig and gerbil brain: a comparative autoradiographic study. Neuropharmacology 40:242–253.

Maggi CA (1995) The mammalian tachykinin receptors. Gen Pharmacol 26:911–944.

Mai JK, Voss T, Paxinos G (2008) Atlas of the human brain. Amsterdam: Elsevier/Academic Press.

Malherbe P, Knoflach G, Hernandez MC, Hoffmann T, Schnider P, Porter RH, Wettstein JG, Ballard TM, Spooren W, Steward L (2011) Characterization of RO4583298 as a novel potent, dual antagonist with in vivo activity at tachykinin $NK_1$ and $NK_3$ receptors. Br J Pharmacol 162: 929–946.

Marco N, Thirion A, Mons G, Bougault I, Le Fur G, Soubrié P, Steinberg R (1998) Activation of dopaminergic and cholinergic neurotransmission by tachykinin $NK_3$ receptor stimulation: an in vivo microdialysis approach in guinea pig. Neuropeptides 32:481–488.

Meltzer HY, Arvanitis L, Bauer D, Rein W (2004) Placebo-controlled evaluation of four novel compounds for the treatment of schizophrenia and schizoaffective disorder. Am J Psychiatry 161:975–984.

Mikula S, Trotts I, Stone J, Jones EG (2007) Internet-enabled high-resolution brain mapping and virtual microscopy. NeuroImage 35:9–15.

Mileusnic D, Lee JM, Magnuson DJ, Hejna MJ, Krause JE, Lorens JB, Lorens SA (1999) Neurokinin-3 receptor distribution in rat and human brain: an immunohistochemical study. Neuroscience 89:1269–1290.

Nagano M, Saitow F, Haneda E, Konishi S, Hayashi M, Suzuki H (2006) Distribution and pharmacological characterization of primate NK-1 and NK-3 tachykinin receptors in the central nervous system of the rhesus monkey. Br J Pharmacol 147:316–323.

Nagy K, Tóth M, Major P, Patay G, Egri G, Häggkvist J, Varrone A, Farde L, Halldin C, Gulyás B (2013) Performance evaluation of the small-animal nanoScan PET/MRI system. J Nucl Med 54:1825–1832.

Nalivaiko E, Michaud JC, Soubrie P, Le Fur G, Feltz P (1997) Tachykinin neurokinin-1 and neurokinin-3 receptor-mediated responses in guinea-pig substantia nigra: an in vitro electrophysiological study. Neuroscience 78:745–757.

Pantaleo N, Chadwick W, Park SS, Wang L, Zhou Y, Martin B, Maudsley S (2010) The mammalian tachykinin ligand-receptor system: an emerging target for central neurological disorders. CNS Neurol Disord Drug Targets 9:627–635.

Rapisarda C, Bacchelli B (1977) The brain of the guinea pig in stereotaxic coordinates. Arch Sci Biol 61: 1–37.

Rigby M, O'Donnell R, Rupniak NM (2005) Species differences in tachykinin receptor distribution: further evidence that the substance P ($NK_1$) receptor predominates in human brain. J Comp Neurol 490:335–353.

Sarau HM, Griswold DE, Bush B, Potts W, Sandhu P, Lundberg D, Foley JJ, Schmidt DB, Webb EF, Martin LD, Legos JJ, Whitmore RG, Barone FC, Medhurst AD, Luttmann MA, Giardina GA, Hay DW (2000) Nonpeptide tachykinin receptor antagonists. II. Pharmacological and pharmacokinetic profile of SB-222200, a central nervous system penetrant, potent and selective NK-3 receptor antagonist. J Pharmacol Exp Ther 295:373–381.

Seabrook GR, Bowery BJ, Hill RG (1995) Pharmacology of tachykinin receptors on neurones in the ventral tegmental area of rat brain slices. Eur J Pharmacol 273:113–119.

Spooren W, Riemer C, Meltzer H (2005) Opinion: $NK_3$ receptor antagonists: the next generation of antipsychotics? Nat Rev Drug Discov 4:967–975.

Szanda I, Mackewn J, Patay G, Major P, Sunassee K, Mullen GE, Nemeth G, Haemisch Y, Blower PJ, Marsden PK (2011) National Electrical Manufacturers Association NU-4 performance evaluation of the PET component of the NanoPET/CT preclinical PET/CT scanner. J Nucl Med 52:1741–1747.

Tooney PA, Au GG, Chahl LA (2000) Localisation of tachykinin NK1 and NK3 receptors in the human prefrontal and visual cortex. Neurosci Lett 283:185–188.

Topaloglu AK, Semple RK (2011) Neurokinin B signalling in the human reproductive axis. Mol Cell Endocrinol 346:57–64.

Varrone A, Sjöholm N, Eriksson L, Gulyás B, Halldin C, Farde L (2009) Advancement in PET quantification using 3D-OP-OSEM point spread function reconstruction with the HRRT. Eur J Nucl Med Mol Imaging 36:1639–1650.

Yilmazer-Hanke DM (2012) Amygdala. In: The human nervous system, 3rd edition (Mai JK and Paxinos G, eds), pp759–834. San Diego: Elsevier Academic Press.